Correlation between microstructure and charge transport in poly(2,5-dimethoxy-*p*-phenylenevinylene) thin films

M. Sims,* S. M. Tuladhar, J. Nelson, R. C. Maher, M. Campoy-Quiles, S. A. Choulis, M. Mairy, and D. D. C. Bradley†
Experimental Solid State Physics Group, The Blackett Laboratory, Imperial College London, Prince Consort Road, London SW7 2BZ, United Kingdom

P. G. Etchegoin
The MacDiarmid Institute for Advanced Materials and Nanotechnology, School of Chemical and Physical Sciences, Victoria University of Wellington, P.O. Box 600, Wellington, New Zealand

C. Tregidgo, K. Suhling, and D. R. Richards
Department of Physics, King's College London, Strand, London WC2R 2LS, United Kingdom

P. Massiot, C. B. Nielsen, and J. H. G. Steinke
Department of Chemistry, Imperial College London, South Kensington Campus, London SW7 2AZ, United Kingdom
(Received 19 March 2007; revised manuscript received 16 July 2007; published 19 November 2007)

We report a study of thin films of poly(2,5-dimethoxy-*p*-phenylenevinylene) (PDMeOPV) prepared by a precursor route. Conversion at two different temperatures, namely, 120 and 185 °C, produces *partially* and *fully* converted films. We study the structural, optical, and charge transport characteristics of these samples in order to relate transport properties to microstructure. Micro-Raman mapping and photoluminescence (PL) imaging reveal the existence of coarse, depth-averaged domains of around 50 μm in lateral extent, with more pronounced contrast for conversion at the higher temperature. The contrast in both micro-Raman and PL maps can be attributed to fluctuations in film density. Spectroscopic ellipsometry studies of the films indicate that the average film density is approximately 15% higher for conversion at the higher temperature. Time-of-flight photocurrent transients, recorded here in PDMeOPV films, are typically dispersive but yield hole mobilities in excess of 10^{-4} $cm^2/V\,s$ at modest applied fields ($\sim 1.2\times 10^5$ V/cm) in the fully converted films. To our knowledge, these are amongst the highest reported mobility values for a poly(*p*-phenylenevinylene) derivative. Fully converted films, while yielding higher hole mobilities, exhibit a stronger dependence on electric field than partially converted ones. The higher mobility can be attributed to the almost complete conversion of the flexible saturated subunits within precursor chains to conjugated vinylene moieties at elevated temperature. This results in a correspondingly higher packing density, an improvement in intrachain transport, and a reduction in the smallest interchain hopping distance. We suggest that the stronger electric field dependence is due to the increasing influence of intermolecular electrostatic interactions with decreasing interchain separation. We propose that a greater proportion of chains in the fully converted films packs in a three-dimensional, interdigitated arrangement similar to that described previously for crystalline samples of PDMeOPV [J. H. F. Martens *et al.*, Synth. Met. **55**, 449 (1993)].

DOI: 10.1103/PhysRevB.76.195206 PACS number(s): 73.61.Ph, 61.41.+e, 78.30.Jw

I. INTRODUCTION

Conjugated polymers are of increasing interest as new materials for electronic applications offering the potential for low fabrication cost, easy processing, and flexibility. Organic light emitting diodes (OLEDs),[2] field effect transistors (FETs),[3] photodiodes,[4] and solar cells[5] are all applications under intense study with the first products already emerging. One of the limitations for the utilization of such organic semiconductors is that they have relatively poor carrier transport properties. Low mobilities can limit practical applications: For instance, the use of OLEDs in passive matrix addressed displays is limited by the typically low current density that arises in the space-charge-limited current regime. Low mobility also impacts on switching speed in FETs and on solar cell efficiency. Conjugated polymers with enhanced carrier transport are, therefore, much needed for optimization of organic electronic devices.[6,7]

Poly(*p*-phenylenevinylene) (PPV) derivatives have been widely studied over recent years.[8–14] They tend to have relatively low hole mobilities compared to other conjugated polymers such as polyfluorenes[6] and polythiophenes.[7] Alkoxy substitution of the phenylene group lowers the energy gap associated with the phenylenevinylene backbone, making alkoxy PPVs relatively attractive compounds for organic solar cell development.[9] This has prompted particular interest in learning to understand and ultimately control the charge transport properties of this material set. Variations in mobility of over an order of magnitude have been observed in dialkoxy PPVs as a result of different solvents,[9,10,13] side-chain variation,[12] the application of an electric field during film deposition,[11] or annealing.[9,14] These differences are normally attributed to intrinsic factors, particularly changes in chain packing. It is important to note, however, that extrinsic factors such as chemical purity also have a marked impact on charge mobility, as was recently demonstrated with the ob-

servation of ambipolar transport in a highly purified regioregular polythiophene derivative.[7] Indeed, it is still unclear to what extent, if at all, the prevalent hole transport (and often immeasurable electron mobility) often associated with PPV derivatives is attributable to intrinsic properties of the polymer electronic structure rather than to chemical purity. In order to develop molecular materials with improved transport properties, new techniques are needed to distinguish the relative roles of intrinsic polymer properties (e.g., conformation, packing, and polaron binding energy) and extrinsic factors in determining the nature of charge transport and the resulting mobilities. In this respect, simple optical probes that can provide information on chain packing within solution-cast thin films would be extremely valuable, especially if they could be used without the requirement for device fabrication and without the stringent requirements, such as uniformity, needed for microstructural probes such as x-ray diffraction. In this paper, we address the relationship between microstructure and charge transport in a semicrystalline, symmetrically substituted dialkoxy-PPV derivative, namely, poly(2,5-dimethoxy-*p*-phenylenevinylene) (PDMeOPV). Using this polymer as a model system, we also show how spatially resolved photoluminescence and Raman spectroscopy can indeed be used to probe the structural properties of polymer thin films.

PDMeOPV has previously been shown to adopt a highly crystalline three-dimensional packing within suitably processed films.[1,15] Freestanding aligned films, stretch oriented during the conversion reaction, and ultrathin films cast and converted on, and subsequently floated off, KBr crystal plates show, respectively, well defined x-ray and electron diffraction patterns. This contrasts somewhat with the case for unsubstituted poly(*p*-phenylenevinylene) (PPV), in which strong two-dimensional ordering occurs [crystallographic *c* (intrachain) and *b* axes], but with an axial translational disorder of the (100) planes.[16–18] The improvement in chain packing relative to PPV has been rationalized by an interdigitation in the *a* direction of methoxy groups on adjacent molecules.[1,15] Analysis of reflections from stretched samples indicates separation distances as low as a 3.6 Å between chains.[15] Such ordering is facilitated by a coplanar sawtooth profile of the individual molecules, which is stabilized by H bonding between the oxygen atoms and methyl groups on adjacent monomeric units. The amount of translational disorder that can occur along the *a* axis is correspondingly restricted. Apart from ensuring good registration, interdigitation promotes long-range order: For instance, transmission electron microscopy studies using a 100 μm^2 beam cross section have revealed single crystal electron diffraction patterns for the ultrathin PDMeOPV films converted on KBr plates.[19] These desirable structural characteristics can, in turn, be expected to facilitate improved charge carrier mobilities, providing a key motivation for our current study.

Little is known to date about the transport characteristics of PDMeOPV. This may be due, in part, to the difficulties of fabricating PDMeOPV films on indium tin oxide (ITO) coated substrates. Corrosion of the ITO anode is an expected result of the acidic atmosphere that is required during thermal conversion of the methoxy leaving group precursor (see Fig. 1). We have overcome this problem by developing a

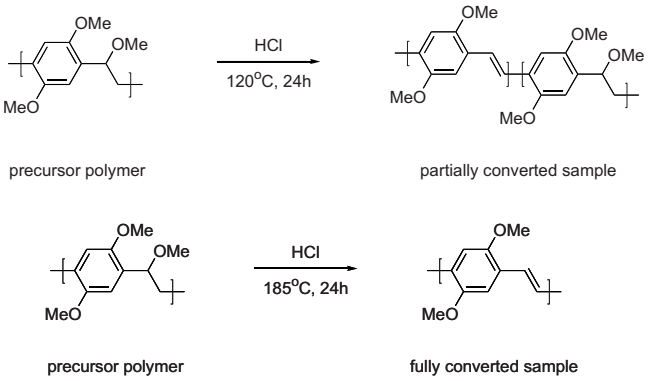

FIG. 1. Conversion routes to partially and fully converted films of poly(2,5-dimethoxy-*p*-phenylenevinylene) (PDMeOPV).

method to produce device structures from freestanding PDMeOPV films, enabling us to explore the charge transport properties of this insoluble conjugated polymer.

We compare films of PDMeOPV that have been converted at different temperatures, classified here as *partially* and *fully* conjugated samples (see Sec. II for preparation details). As we shall show, the different conversion temperatures lead to very different morphologies and optoelectronic properties. We access information on charge transport properties using time-of-flight (TOF) mobility measurements, and we show that fully converted samples exhibit higher hole mobilities and a stronger dependence of mobility on electric field than partially converted samples. We then compare the microstructure of the partially and fully converted films using Raman and photoluminescence (PL) spectroscopy. Micro-Raman maps and micro-PL images reveal domains with sizes of the order of ~50 μm for both sample types, but the fully converted samples exhibit greater contrast (larger spread in the mapping parameters). This greater contrast is consistent with a higher average chromophore number density (closer chain packing), an attribute that should indeed arise from more complete elimination of the precursor's flexible saturated segments. The higher chromophore density is confirmed using spectroscopic ellipsometry, and the correlation between microstructure and charge transport is then discussed in terms of chain packing, intermolecular interactions, and hopping distances. Besides the demonstration of unusually high charge carrier mobilities for a PPV derivative, an important outcome of our work is the establishment of spatially resolved PL and Raman measurements as effective local probes of structural heterogeneity in polymer films with spectroscopic ellipsometry measurements providing a useful consistency check. These latest results complement our earlier studies in which we have used such optical probes to monitor thermal transition temperatures and to characterize the state of order within oriented conjugated polymer thin films.[20]

II. SAMPLE PREPARATION AND EXPERIMENTAL DETAILS

Details of the synthetic route to the precursor can be found elsewhere.[21] Freestanding PDMeOPV films with

thickness $d \approx 1.2$ μm were prepared as follows. Precursor polymer films (see Fig. 1 for chemical structure) were spin coated (900 rpm) from dichloromethane solution (76 mg/ml) onto freshly pressed anhydrous potassium bromide (KBr) disks. The precursor samples were placed within an airtight chamber within which they were converted by being heated while simultaneously exposed to a continuous gas stream carrying HCl vapor (a catalyst for the removal of the methoxy leaving group). In order to minimize the prospect of carbonyl formation in competition with the formation of a conjugated vinylene link, the carrier gas (bubbled through an HCl reservoir on its way into the chamber) was selected to be a 95:5 nitrogen:hydrogen reducing gas mixture.[22]

Partially converted films were prepared by heating for 24 h at 120 °C under forming gas/HCl. This temperature lies below the glass transition temperature $T_g \approx 185$ °C, determined for the precursor polymer by differential scanning calorimetry (heating is then performed without the HCl conversion catalyst): Significant morphological change is not therefore expected to occur under these conditions. Conversion in this way results in the initially colorless precursor films turning a deep orange color, as expected for the formation of conjugated vinylene linkages that extend the conjugation length, and consistent with Fourier transform infrared (FTIR) analysis that showed an approximate 80% reduction in absorption at 1093 cm^{-1} (non-aromatic O-CH_3 stretch).

Fully converted films were prepared by heating at 185 °C under forming gas/HCl. In an attempt to maximize the resulting crystallinity, the precursor films were first annealed at 190 °C (i.e., above T_g) for 30 min on a Linkam hot stage under a N_2 atmosphere (with no HCl catalyst) and then cooled slowly at a rate of 0.2 °C/min to room temperature. X-ray diffraction analysis revealed that this protocol resulted in highly crystalline (~60%) precursor films. These annealed films were then fully converted (resulting in a complete loss of the 1093 cm^{-1} stretch mode absorption) by heating at 185 °C [below the melting point of the precursor crystallites (>200 °C)] for 24 h under forming gas/HCl as described above. Both full and partial conversion protocols resulted in a ~50% reduction in film thickness. Attempts to convert the crystalline precursor film samples at 120 °C under forming gas/HCl were unsuccessful with negligible change apparent in the FTIR intensity at 1093 cm^{-1}, even after heating for 20 h. It is possible that the crystallites inhibit acid percolation through the film and/or that methanol elimination to form a vinylene double bond is sterically hindered. A temperature of 185 °C was finally selected as a suitable compromise conversion temperature, on the basis that proximity to the initial glass transition temperature would tend to assist the chain rearrangement most likely needed for leaving group elimination, yet largely leaves the crystalline morphology of the precursor film unaltered. Choosing this temperature was not entirely straightforward since T_g can be expected to rise as the conversion reaction proceeds, due to a gradual conjugation-induced stiffening of the backbone. Further process adjustments might therefore be of interest in the future.

For both PDMeOPV sample types, semitransparent aluminum electrodes ($d \sim 30-40$ nm) were evaporated on top of the converted films at a typical pressure of 10^{-6} mbar. The films were then floated off their KBr substrates in de-ionized water, rigorously washed, and dried at room temperature. The device structures for TOF photocurrent measurements were finally completed by thermal evaporation of six shadow-masked, aluminum electrodes (area ~ 4.5 mm^2, $d \sim 100$ nm) on the opposite side of the film. Film thicknesses were measured with a Sloan Dektak™ surface profilometer, and we estimate an accuracy of 5% in these values.

TOF photocurrent transients were measured at room temperature for a range of applied biases under pulsed (6 ns) Nd:YAG (yttrium aluminum garnet) laser (Quantel) excitation through the semitransparent aluminum electrode. Measurements were generally performed at 532 nm using the frequency-doubled laser output, but additional measurements were also made for a subset of structures using the frequency-tripled laser output (355 nm): No discernible difference was observed in the extracted quantities following excitation at 532 and 355 nm. The resulting photocurrent was detected with a digital oscilloscope (Tektronix TDS 3052). The samples were stored *in vacuo* and measured both *in vacuo* and under ambient conditions without any observed difference in the hole mobility values. The laser pulse intensity was controlled so that the charge generated did not exceed 10% of the product of the capacitance C of the sample and the applied voltage V. This allowed us to assume a constant electric field across the samples. The carrier transit time t_{tr}, defined as the time required for the photocarriers to travel across the film thickness d, was determined at each applied bias from the intersection point of the short-time and long-time asymptotes to double-logarithmic plots of current versus time. Hole mobilities μ were deduced from these values via

$$\mu = \frac{d^2}{t_{tr} V}. \tag{1}$$

The mobility measurement was repeated at a range of applied biases representing electric fields between 1.5×10^5 and 1.0×10^6 V/cm. Temperature dependent measurements were carried out in a nitrogen-filled cryostat at temperatures in the range from ~210 to ~310 K.

Absorption spectra were measured with a Unicam 4 UV-visible spectrophotometer. Thin films ($d \sim 90$ nm) were prepared for the measurements by spin coating onto Spectrosil B substrates followed by either partial or full conversion as described above. Photoluminescence (PL) spectra were excited at ~450 nm (excitation area ~4 mm^2) by normal incidence exposure of the sample to a monochromated Bentham xenon lamp, and the emission was collected with a silica fiber bundle held at ~45° to normal incidence, spectrally dispersed with a spectrograph and detected with an Instaspec IV cooled charge-coupled device (CCD). All spectra were corrected for the power response of the detection system.

Spatially resolved PL measurements were made using an inverted confocal scanning microscope (Leica TCS SP2). Samples (spin coated onto silicon substrates from the same solutions and using the same spin conditions as were used for the TOF devices) were excited by the 488 nm line of an

Ar^+ laser via a ×63 water immersion objective (numerical aperture=1.2). The PL was dispersed spectrally by a prism and detected with a photomultiplier tube. A wavelength-resolved stack of images (238×238 μm^2, 512×512 pixels) was collected with 5 nm resolution in 5 nm intervals.

Raman measurements were made on a Renishaw 2000 CCD-based instrument equipped with a BH-2 confocal microscope and a Prior mapping stage, using a 20 mW 780 nm near infrared diode laser excitation source. The laser light was focused onto the sample with a ×50 objective to produce a beam of diameter of ≈1 μm at the focal point. Raman maps (1 μm resolution, 0.1 second integration time) were obtained over 251×251 μm^2 areas for each sample. The Raman peaks were analyzed (Curvefit for GRAMS and ORIGIN) using mixed Gaussian and Lorentzian fits (Voigt) with a subtracted background.

Variable angle spectroscopic ellipsometry was carried out using a SOPRA rotating polarizer ellipsometer. Films were spin coated onto Spectrosil B fused quartz substrates. The data were collected for three incidence angles of 62°, 60°, and 58° with respect to the surface normal. The wavelength was scanned from 650 to 850 nm in 4 nm steps. A Cauchy law was employed to analyze the ellipsometry data in order to deduce the dispersion of the refractive index in the transparency region of the polymer. The refractive index at wavelengths (850 nm in this case) far to the red of the longest wavelength electronic transition peak was used to examine the changes in average film density (ρ) using the formula[23]

$$\frac{n_{full}^2-1}{n_{partial}^2-1}\cong\frac{\rho_{full}}{\rho_{partial}}, \tag{2}$$

which is based on the assumption that there is no significant change in the transition matrix element between partially and fully converted samples. This assumption seems reasonable since only some 5–10 conjugated segments are needed in sequence to bestow most of the optical attributes of a long chain poly(arylenevinylene) sample (in part due to conformational distortions that limit conjugation length within longer sequences).[24]

III. RESULTS

A. Time-of-flight hole mobility

Typical hole photocurrent transients for the fully converted (filled circles) and partially converted (open circles) structures, plotted on double-logarithmic axes, are presented in Fig. 2(a). While the transport is relatively dispersive, a clear change in gradient of the photocurrent-time plot is observed in both the transients at ~10 and 37 μs after laser excitation for the fully and partially converted samples, respectively. The lack of a plateau region between the point of charge carrier generation and charge collection at the aluminum anode indicates that the carriers do not attain a uniform drift velocity during their motion across the film. This dispersive behavior is normally assigned to a wide range of charge hopping rates and is consistent with the observation of a large spread of recombination rates for the charged species in photoinduced absorption studies reported previously.[25] Comparison of a large number of photocurrent transients showed that fully converted samples usually showed more dispersive behavior than partially converted samples.

The electric field dependence of the room-temperature hole mobility is shown in Fig. 2(b). Poole-Frenkel-type behavior is observed for both samples, with the field dependence being approximately twice as strong for the fully converted film. Measurements of thickness for both the fully and partially converted samples (d=1.2 μm) yielded values that were indistinguishable within errors (~5%). The hole mobility in the fully converted film (3.0×10^{-4} $cm^2/V\,s$) at an applied field of 2.1×10^5 V/cm is approximately 25 times higher than in the partially converted film (1.2×10^{-5} $cm^2/V\,s$). The observed field trends indicate that this difference should increase at higher electric fields, but the transit times for the fully converted film at high fields become too short for detection with our setup. The deduced hole mobility in the fully converted film is a relatively high room-temperature TOF mobility for a conjugated polymer and is higher than any mobility previously reported for a poly(p-phenylenevinylene) (PPV) derivative.

The hole mobility in both film types was measured at temperatures between ~210 and ~310 K [Fig. 2(c)] in order to compare the hole transport behavior in more detail. The data in Fig. 2(c) confirm that the hole mobility in the fully converted film exceeds that in the partially converted film over the whole range of temperatures. While the dependence on temperature is similar for both films and is similar to that reported previously for PPV derivatives,[12,26] the dependence on electric field is more positive for the fully converted sample.

Several frameworks, such as the Gaussian disorder model[27] (GDM) and its variants, have been used to analyze the field and temperature dependences of mobility in disordered semiconductors. However, those models are developed for systems where the variations in site energy disorder and electronic coupling can be assumed to be isotropic, whereas in the present case, as we shall show, the films are characterized by large lateral structural heterogeneities. The parameters obtained by a GDM analysis of these samples would not relate to transport parameters within the different domains in the films and would therefore have no useful physical meaning. Here, we simply comment that, in agreement with most physical pictures of charge transport in organic semiconductors, the dispersive photocurrent transients and strong dependence on temperature observed for these samples are indicative of significant disorder in hopping site energies. The larger magnitude of mobility for the fully converted sample indicates that the mean electronic coupling in those parts of the film responsible for hole transport increases upon full conversion.[28] In addition, the different dependence on electric field between the samples may be related to a different degree of disorder in the electronic coupling between hopping sites.

B. Raman spectroscopy and micro-Raman maps

We have previously reported on how Raman spectroscopy can be used to probe local order in conjugated polymer

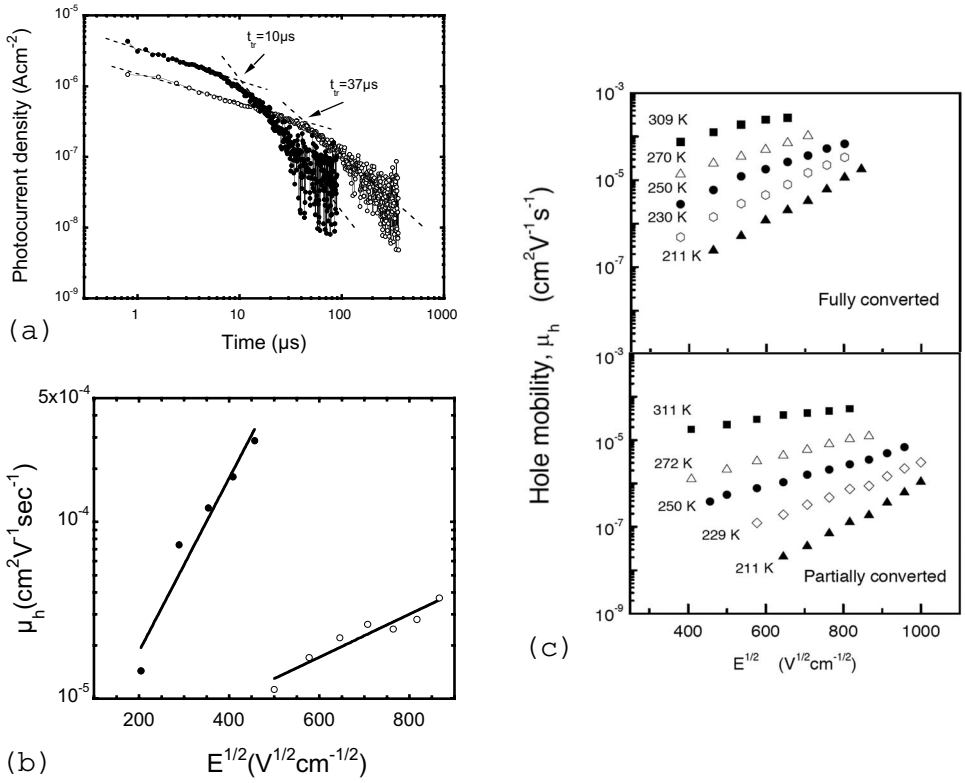

FIG. 2. (a) Typical room-temperature TOF photocurrent transients (at $E=2.4\times10^5$ V/cm) for fully (filled circles) and partially (empty circles) converted freestanding PDMeOPV films ($d=1.2$ μm). Note that the data are displayed on a double-logarithmic plot. The corresponding transit times t_{tr} are marked on the plot: t_{tr} is reduced from 37 to 10 μs, respectively, on going from the partially to the fully converted sample. (b) Electric field dependence of the room-temperature hole mobility in partially (empty circles) and fully converted PDMeOPV free standing films ($d=1.2$ μm). The data are plotted as a function of the square root of the external electric field. Each data point was determined from the intersection of the asymptotes to the corresponding double-logarithmic photocurrent transient plots. (c) Temperature and electric field dependences of hole mobility for the fully (upper panel) and partially (lower panel) converted films.

films.[29] Broadly speaking, Raman is well suited in probing the internal structure of films with thicknesses on the order of 1 μm (as used for TOF measurements). As the focal depth of the confocal Raman microscope at nonresonant wavelengths (e.g., the 780 nm excitation used here) is expected to be of the order of or comparable to the film thickness (at best),[29(a)] Raman scattering can provide information from below the film surface. This is particularly important for polymer systems, which are known to be able to adopt structures at both the bound and air interfaces that are distinct from the bulk structure.[29(b)]

Corresponding Raman spectra (not normalized) for the fully converted sample, collected from two distinct regions on the TOF sample (in gaps between metallized areas), are given in Fig. 3(a). The 1581 cm^{-1} mode is the strongest component amongst a triplet of carbon-carbon stretching modes in the 1500–1600 cm^{-1} range and is identified as a stretching mode of the dimethoxy-substituted phenylene rings.[30] A similar mode occurs in all phenylene containing polymers, but its wave number can vary, for example, in PPV, it is found at 1586 cm^{-1}. The weaker intensity, higher wave number carbon-carbon stretching mode at 1621 cm^{-1} corresponds to the 1628 cm^{-1} mode in PPV and is assigned to a C=C stretching mode of the vinylene linkage between neighboring phenylene rings. This mode tends to decrease in intensity relative to the stronger carbon-carbon ring-stretching mode as the sample conjugation length increases, an observation that is consistent with the observed behavior for fully converted and partially converted PDMeOPV samples [see Fig. 3(b)].

The ≈1280 cm^{-1} mode is one of the doublet of modes that is assigned to in-plane vibrations involving a mixture of C-C/C=C stretching and C-H bending motions. Similar modes have been reported for poly [2-methoxy-5-(2′ethyl-hexoxy)-1,4-phenylene-vinylene] (1290 and 1318 cm^{-1}),[31] and PPV (1301 and 1329 cm^{-1}),[32] although in the latter case, the lower wave number component is very weak. A close relationship between the origins of these two modes is consistent with the observation that the ratio of their intensities remained constant during lateral line scans across film samples (discussed further below). On the other hand, we found that the ≈1581 cm^{-1} ring-stretching mode displays a considerable intensity variation relative to the doublet when measured at different locations on a sample. We return to this point below.

As noted above, the spectra in Fig. 3 show that the relative intensity of the ring-stretching mode at ≈1581 cm^{-1} compared to the in-plane mode at ≈1280 cm^{-1} depends on the precise film location at which the spectra are collected. In order to investigate this dependence further, lateral scans were performed across 500 μm linear stretches of film. Figure 4(a) shows 500 μm line scans for the fully converted

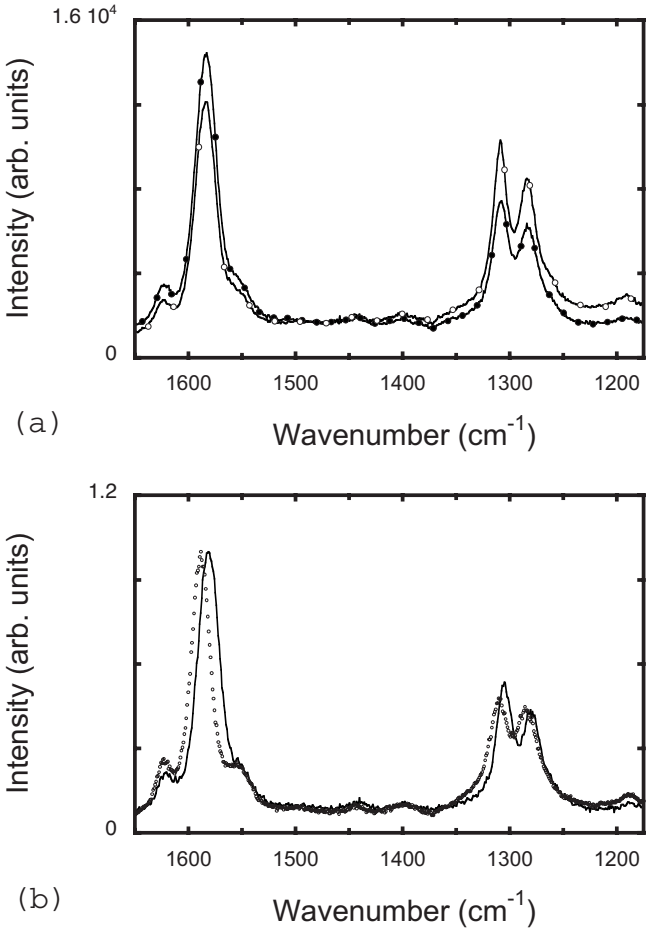

FIG. 3. (a) Representative Raman spectra ($\lambda_{ex}=780$ nm) showing the dominant backbone modes discussed in the main text. The spectra were taken in a bright (empty circles) and a dark (filled circles) region of the map of the fully converted PDMeOPV TOF sample [see Fig. 5(a)]. (b) Raman spectra showing the principal Raman modes for both a fully (solid line) and a partially (empty circles) converted film. The spectra have been normalized to the ring-stretching mode ($\sim$1581 cm^{-1}) intensity. The observed softening of the backbone modes and weakening of the vinylene C=C stretch intensity (1621 cm^{-1}) in fully converted samples is consistent with an increase in effective conjugation length.

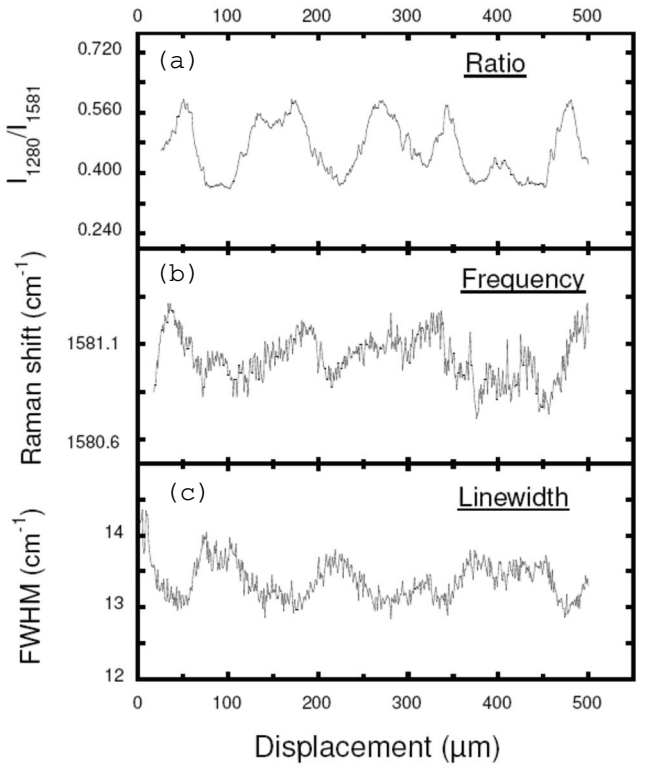

FIG. 4. 500 μm length scans for the fully converted PDMeOPV TOF sample ($d=1.2$ μm) showing (a) the ratio of the intensity of the $\approx$1280 cm^{-1} backbone mode to that of the $\approx$1581 cm^{-1} quadrant ring-stretch mode, (b) the peak wave number of the quadrant ring-stretch mode, and (c) the FWHM of the quadrant ring-stretch mode.

sample of the ratio (I_{1280}/I_{1581}) of the Raman intensities of the lower wave number component ($\approx$1280 cm^{-1}) of the in-plane doublet and the principal ring-stretching mode ($\approx$1581 cm^{-1}) and [Figs. 4(b) and 4(c)] the frequency and corresponding full width at half maximum (FWHM) linewidth of the latter $\approx$1581 cm^{-1} mode. Our choice of these particular modes was based on their relative strength (they are among the strongest modes within the spectrum of PDMeOPV), which aids the accuracy of the peak fitting process. Figures 4(a) and 4(c) show that regions with a higher I_{1280}/I_{1581} Raman intensity ratio possess lower FWHM values for the 1581 cm^{-1} mode. Furthermore, in regions with a reduced FWHM, the ring-stretching mode tends to shift to slightly higher wave number [Fig. 4(b)]. A similar correspondence (narrowing and hardening) is observed for both the 1280 and 1305 cm^{-1} modes (not shown).[33] The full extent of the frequency shift is limited to $\sim$0.4 cm^{-1}, considerably smaller than the $\sim$7 cm^{-1} frequency difference between fully and partially converted samples [see Fig. 3(b)]. This confirms that the contrast in the line scans of Fig. 4 does not simply arise from regions corresponding to different stages of conversion, at least within the lateral resolution limit of $\sim$1 μm. It is notable that the Raman ratio data exhibit a considerable enhancement in signal-to-noise ratio relative to the FWHM and frequency data for the ring-stretch mode. The increased signal-to-noise ratio in combination with a greater contrast identifies the ratio results as providing the most useful data set with which to construct spatial maps of microstructure.[34] Raman intensity ratio maps with a 1 μm spatial resolution over an area of 251×251 μm^2 (63 001 spectra) for the same 1.2 μm thick films used in our TOF structures (measuring at a location close to but remote from that where the electrodes were deposited) are presented for the fully and partially converted samples in Figs. 5(a) and 5(b), respectively. The maps show a considerable microstructure. Statistical analyses of the Raman ratio values yield a mean ratio of 0.568 for the fully converted sample with a standard deviation (σ) of 9.7×10^{-2}. Corresponding values for the partially converted sample are 0.397 with a σ value of 5.8×10^{-2}. The lower standard deviation for the partially converted sample reflects reduced large-scale heterogeneity relative to the fully converted sample and is visible as a contrast reduction in the map. The higher σ value for the fully converted sample is consistent with other observations,

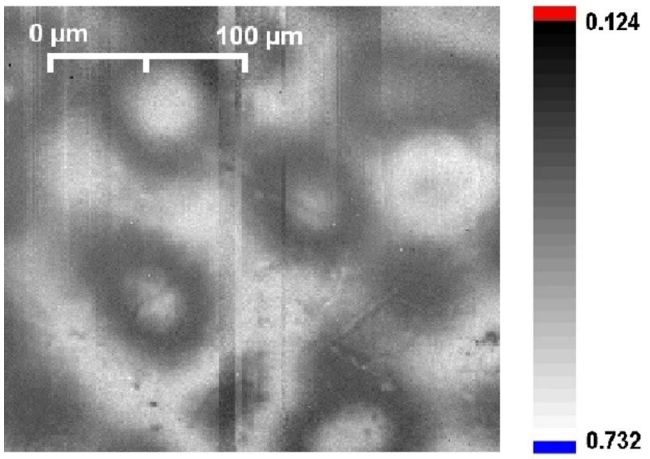

FIG. 5. (Color online) 250×250 μm^2 Raman maps (λ_{ex} =780 nm) displaying the ratio of the intensities of the 1280 and 1581 cm^{-1} modes (see main text for details) for (a) fully converted and (b) partially converted PDMeOPV TOF samples (d=1.2 μm). Lighter shades (higher ratios) correspond to a higher packing density.

namely, the requirement of including a thicker roughness layer to give a good fit to the ellipsometry data (see below) and the more dispersive photocurrent transients for such samples.

C. Photoluminescence spectra and spatial maps

Figure 6 shows the room-temperature optical absorption and PL spectra for a fully converted (solid lines) and a partially converted (dashed lines) spin-coated PDMeOPV film. PL was excited at 450 nm over an area of 1×4 mm^2. The delocalized π-π^* absorption band in the fully converted sample is centered at 448 and at 437 nm in the partially converted sample. The finite blueshift in the latter can be attributed to the existence of residual saturated linkages with their associated leaving group substituents, which will tend to both lower the average conjugated segment length and

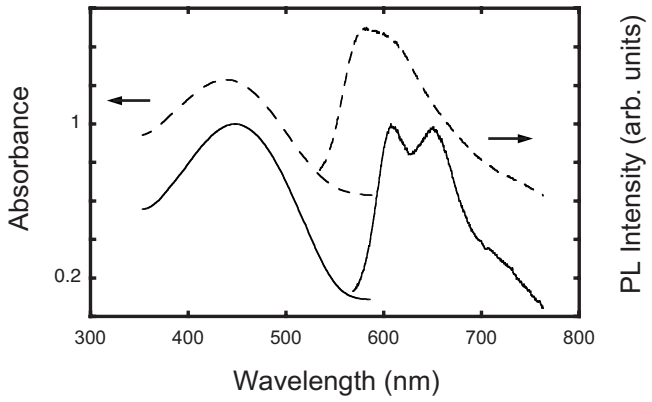

FIG. 6. UV-visible absorption and photoluminescence spectra for fully converted (solid line) and partially converted (dashed line, displaced vertically for clarity) spin-coated PDMeOPV films. Absorption spectra were obtained for films (d=90 nm) spin coated onto fused quartz Spectrosil B substrates. The PL spectra correspond to relatively thick films (d=1.2 μm) spin coated onto KBr substrates. FWHM values for the PL spectra are 0.30 and 0.39 eV for the fully and partially converted samples, respectively.

frustrate the adoption of a planar extended chain conformation. This is consistent with the observation of a somewhat lower absorbance in partially converted samples (reduced π-electron conjugation). We measured peak absorption coefficients of $\sim9.4\times10^4$ cm^{-1} for fully converted samples and $\sim5.1\times10^4$ cm^{-1} for partially converted samples.

The corresponding PL data show more pronounced spectral differences. Clear vibronic structure is evident in the fully converted sample, with two dominant modes (identified, respectively, as S_1 to S_0 0-0 and 0-1 transitions) located at 608 and 651 nm, respectively. There is also a shoulder at longer wavelength ($\approx$720 nm). In contrast, the PL spectrum of the partially converted sample shows no resolved vibronic structure and it is substantially blueshifted (peak near 580 nm) relative to the fully converted sample.

The differing shapes of the PL spectra for the two conversion temperatures are consistent with the idea that the sample converted at the lower temperature (120 °C) retains a significant proportion of unconverted repeat units. Normally, spectral diffusion in a conjugated solid ensures that PL originates from the lowest energy chromophores (i.e., longest conjugation length segments) and exhibits vibronic structure characteristic of these low energy segments.[35] The absence of resolved vibronic structure (or equivalently the presence of large PL linewidths) can be the result of a wide distribution of exciton hopping times in a disordered system.[36] As disorder increases, time constants for exciton hopping increase and radiative exciton decay begins to compete with exciton hopping. In the limit of very slow exciton diffusion, radiative decay, on average, occurs before diffusion and the emission spectrum then reflects the whole ensemble of absorbing site energies, resulting in closer mirror symmetry between absorption and emission spectra. In the present case, the loss of vibronic structure in the partially converted sample appears entirely consistent with an inhibition of exciton hopping by the residual saturated linkages and lower degree of orientational order within the polymer chains in the

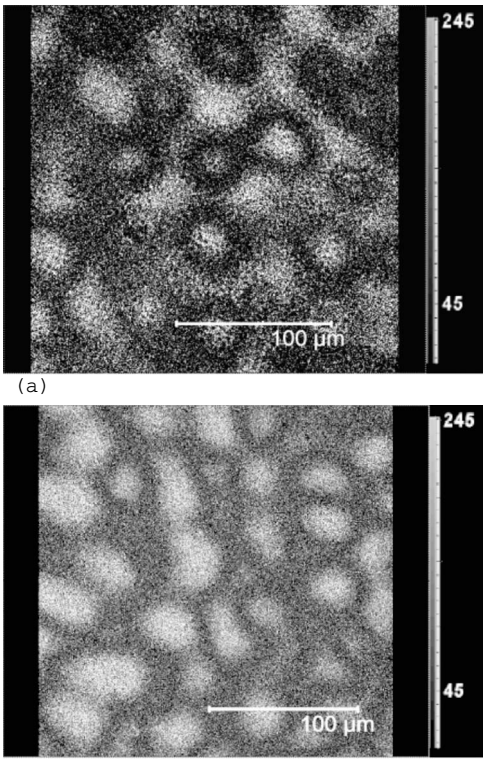

FIG. 7. 238×238 μm^2 PL micrographs displaying the ratio of the PL intensity detected at 660 nm to that detected at 600 nm for (a) fully converted and (b) partially converted PDMeOPV films spin coated onto silicon substrates. The samples were spin coated from the same solution used to prepare the TOF devices, and they were excited in a region close to the substrate.

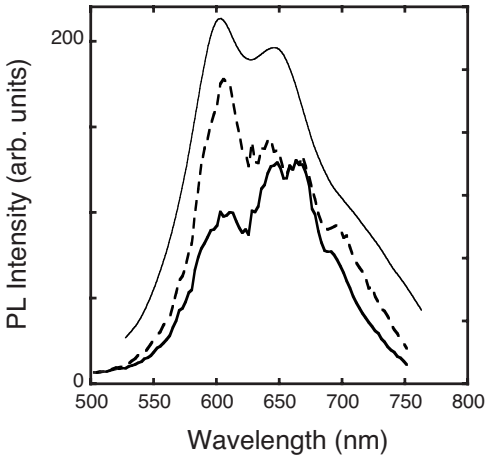

FIG. 8. Representative PL spectra (not normalized) collected at two different locations on a fully converted PDMeOPV sample spin coated onto a silicon substrate. The spectra were taken at locations corresponding to the bright (full line) and dark (dashed line) regions of the PL map shown in Fig. 7(a). The excitation wavelength was 488 nm. A standard (excited over an area of 4 mm^2) PL spectrum for a fully converted film, spin coated onto a Spectrosil B fused quartz substrate, is also shown but offset vertically for clarity.

film. This would also explain the observed blueshift in emission, since the residual methoxy leaving groups will disrupt conjugation (both chemically and conformationally) and thus reduce the average extension of the emitting chromophores.

Spatial mapping of the PL emission has been performed on a micron length scale via scanning confocal microscopy. Images acquired by near-surface excitation showed no significant spectral variations for either the fully or partially converted samples. However, deeper focus data yielded redshifted spectra in some regions: This is visualized by mapping the ratio of the PL intensity detected at 660 and 600 nm for the fully and partially converted samples [Figs. 7(a) and 7(b), respectively, wherein the images are normalized and presented on the same full-scale intensity range]. Darker areas represent a relative emission enhancement at 600 nm, whereas lighter areas represent increased relative emission at 660 nm. Examples of spectra (not normalized) collected from a darker (full line) and from a brighter region (broken line) in the map of Fig. 7(a) are shown in Fig. 8. The strong variation in emission intensity at 600 nm is clearly evident. A standard PL spectrum (excited over a 1×4 mm^2 area) for a fully converted sample (spin coated onto a Spectrosil B fused quartz substrate) has been included in Fig. 8 for reference and offset vertically for clarity. The observed microstructure in the PL ratio largely resembles that found in the Raman maps [Figs. 5(a) and 5(b)] with areas of larger PL ratio corresponding reasonably well with the lighter shaded regions in the corresponding Raman map. This correlation is further supported by statistical analyses that again reveal a higher standard deviation in the PL intensity ratio for the fully converted film ($\sigma=60.1$) than for the partially converted film ($\sigma=48.5$). Finally, we note that, in contrast, the same ratio plots for near-surface excitation showed no significant contrast.

D. Spectroscopic ellipsometry

Analysis of the ellipsometry data using a Cauchy law yielded the dispersion of the refractive index in the transparency spectral region of the polymer. It was found that the inclusion of a roughness layer reduced the standard deviation by more than 50%. The roughness layer was modeled as a Bruggeman mixture of polymer and air with 49.5% and 75% polymer weights given to the partially and fully converted films, respectively. This analysis resulted in a roughness layer thickness of 59 ± 2 nm for the fully converted sample and of 46 ± 2 nm for the partially converted sample. The increase in average film density for the fully converted films relative to partially converted films was estimated from the refractive indices n deduced for each sample at 850 nm using Eq. (2): Values of $n=1.64$ and $n=1.57$ were used for the fully converted and partially converted films, respectively, leading to an estimate of the relative density increase $\Delta\rho\approx15\pm3\%$.

IV. DISCUSSION

The TOF mobility data presented above suggest that the mean electronic transfer integral is higher in the fully converted than in the partially converted films. A higher average transfer integral would result directly from a reduced interchain separation or from a more favorable relative orienta-

tion of the charge transporting units on neighboring chains.[37] We now argue that improved three-dimensional packing of the conjugated units upon full conversion is also consistent with our Raman and PL data.

Previously, we showed that line scans of the depolarization ratio of the principal phenylene stretch mode can be used very successfully to indicate local order, or crystallization, in spin-coated and aligned thin films of poly(9,9-dioctylfluorene) (PFO).[29] In that work, polarization anisotropy relied on the highly uniaxial character of the phenylene ring-stretch mode.[29,38] A similar analysis has been applied here to the frequency and FWHM line scans of the $\sim$1581 cm^{-1} ring-stretching mode. Generally, as the registration between phenylene rings increases, inter-ring interactions stabilize tending to reduce the vibrational linewidth and raise its frequency. In view of this, we can immediately associate those areas with sharper and more energetic spectral features with a higher local density and perhaps with a higher degree of side-chain interdigitation. In a similar manner, owing to a good correspondence with the FWHM and frequency features, the regions of higher Raman ratio can be readily correlated with areas of increased chain packing density.

The empirically observed relationship between the Raman ratio (I_{1280}/I_{1581}) and both the FWHM and frequency of the 1581 cm^{-1} ring-stretch mode remains unexplained. We note, however, that, contrary to the case of spin-coated PFO films, in which molecular alignment distances were found to exceed the size of the sampling area in depolarization measurements ($\approx$1 μm^2), large-scale (approximately micrometers) molecular ordering may not provide the best explanation in this instance. We were unable to detect any visible contrast in the depolarization ratio of the 1581 cm^{-1} mode along an arbitrary 500 μm section. It follows, therefore, that crystallite dimensions for our PDMeOPV samples must be on the submicron length scale, consistent with the $\approx$12 nm crystallite size measured by Martens *et al.*[15] in PDMeOPV films. We suggest that the variation in relative intensity of the 1581 cm^{-1} ring-stretch mode to that of the 1280 and 1305 cm^{-1} modes should be attributed to packing-induced changes in Raman activity. One possible explanation could be the effect of interdigitation on the polarizability of the ring-stretching modes. Another could be its effect on steric interactions. Clarification of the origin of the relative intensity fluctuations for the *p*-phenylene ring-stretch mode in PDMeOPV is likely to be of some general interest as it might provide a measure of the local density and mean interchain separation distances, information that would be useful for a wide range of phenylene containing conjugated polymer films.

The 15% lower average density estimated from ellipsometry analyses on the partially converted sample agrees with a lower average value for the Raman ratio [note darker shade in Fig. 5(b)]. This, in turn, is consistent with a lower packing density and a possible lower degree of crystallization. It is interesting to note at this point the observed softening of the principal ring-stretching mode ($\approx$1581 cm^{-1}) upon full conversion that exists alongside a reduction of the C=C vinylene stretch intensity at 1621 cm^{-1} [Fig. 3(b)]. Both of the latter observations are indicative of an increase in effective conjugation length. Taken together, the above evidence suggests that improved chain packing can be associated with a longer effective conjugation length in PDMeOPV films.

The enhanced 660 nm contribution (relative to that at 600 nm) in the PL collected from the denser regions of the fully converted film [Fig. 7(a)] is not considered to be the result of a packing-induced formation of interchain emissive species (e.g., excimers). This conclusion stems from the clearly observed reduction, for the denser regions, in intensity on the short wavelength side of the PL spectrum (S_1 to S_0 0-0 vibronic transition) (cf. Fig. 8) without the appearance of another emission component. Excimer emission normally results in an overall reduction in the usual PL spectrum and the appearance of a redshifted broadband component. Furthermore, we believe that excimer formation would not be favored by the herringbone crystal-packing configuration adopted by PDMeOPV. Characteristic distances for the proposed unit cell (lattice parameters *a* and *b* in the ranges 10.0–13.4 Å and 5.5–9.4 Å, respectively[15]) are in excess of what is typically required for excimer formation[39,40] and taken in conjunction with restricted excited state configurational relaxation (a lower electron-geometry coupling constant imposed by the crystal lattice), make the formation of excimers an improbable outcome. Indeed, if operative at all in PDMeOPV films, excimer formation would be more favored in disordered, glassy regions where chain segmental mobility should be substantially higher. We therefore suggest that PDMeOPV can be considered a conjugated polymer example in which interacting chains [with sufficient strength to facilitate an increased charge hopping rate and a higher degree of energetic disorder (see below)] do not lead to excimer formation on account of strong geometrical constraints.

The variability in PL spectra originating from regions of different densities (Fig. 8) can be explained as a result of variations in the degree of self-absorption. In accordance with the Beer-Lambert law, which states that absorbance increases linearly with absorber concentration and path length,[40] an enhancement in self-absorption can be expected in regions with a higher chromophore concentration (packing density). However, we also point out that the presence of longer light escape path lengths is a reasonable expectation in higher density regions due to the presence of in-plane crystallite scattering. We have previously shown that scattering by crystallites can frustrate the in-plane waveguiding of PL in PFO films[20(b)] and ultimately lead to a substantial increase in the amount of PL exiting in a direction perpendicular to the film plane. In order to verify this speculation, a number of emission spectra were determined at different depths and at various spatial locations (data not shown). Spectra taken by near-substrate excitation tended to show a stronger quenching of the S_1 to S_0 0-0 vibronic transition in relation to near-surface excitation. The difference tended to be greater in the fully converted films with the effect most pronounced in denser regions. The brighter areas (higher 660 nm to 600 nm intensity ratio) in the PL maps can therefore be explained by the combined effect of increased chromophore density and emission path length in crystallite-rich regions of the film. We further comment that the apparent weakness of the 0-0 vibronic peak with respect to the 0-1 replica in the standard spectrum of Fig. 6, which might oth-

erwise be attributed to a relatively large Huang-Rhys parameter, can be simply the result of scattering-induced self-absorption. Scattering-induced self-absorption can also be used to explain a similar reduction in the relative intensity of the 0-0 transition in crystallized PFO films.[20(b),41] Relative to the standard PL spectrum of Fig. 6, the 0-0 transition intensity is visibly enhanced in Fig. 8. This is considered a result, at least in part, of a relative decrease in self-absorption for the much thinner film used in Fig. 8. As a caveat, we found the PL spectrum of PDMeOPV films to exhibit a significant dependence on, amongst other things, our choice of substrate, although a systematic study of this effect was not carried out.

We now consider whether changes in density of the magnitude estimated above are sufficient to explain the increase in zero-field hole mobility. According to the nonadiabatic Marcus theory, the rate of charge hopping is proportional to the square of the electronic transfer integral t between hopping sites. The transfer integral normally varies exponentially with separation $r, t \sim \exp(-r/r_0)$, where the localization length r_0 is typically in the range 0.03–0.1 nm. In the case of dialkoxy-PPV oligomers, we have shown in a separate study that $r_0 \approx 0.04$ nm.[28] If hopping sites were distributed homogeneously, an increase in density of 15%, as determined via ellipsometry for these films, corresponds to a decrease in the linear hopping distance of 4% for an isotropic system. With a hopping distance of the order of 1 nm and r_0 of 0.04 nm, the intermolecular hopping rate could be increased by a factor of 8 as a result of a 15% density increase alone. Since mobility is expected to be proportional to the hopping rate, this density increase could help to explain the 25-fold difference in hole mobilities at 2.1×10^5 V/cm observed for this system but could not explain the effect entirely. However, if the density increase occurs heterogeneously such that chain packing in the denser regions of the film is increased by significantly more than 15%, then the interchain hopping rates within the denser regions could increase by a much larger factor than expected for a homogeneous densification. In such a heterogeneous system, we expect the fastest interchain hopping points (which will lie in the denser regions of the film) to dominate the mobility since intrachain carrier mobilities are expected to be substantially higher than those for any interchain process. Therefore, the mobility would increase in proportion to the hopping rates in the denser regions of the film, rather than the average rate. The increased heterogeneity observed in the Raman maps of the fully converted compared to the partially converted film supports this mechanism for the mobility increase.

An additional factor that could help explain the much lower hole mobilities in the partially converted film is the presence of a significant number of saturated methoxy units along each chain. The presence of such inert units would result in regions of the film with larger charge hopping distances than might be expected for a given average film density. Such units are also likely both to disrupt the relative orientation of conjugated segments and to reduce the extension of conjugated units along the chain. Such breaks in conjugation can inhibit intrachain charge transport, reducing the ability of carriers to find the optimum interchain hopping points. A positive correlation between intrachain delocalization and net mobility has been observed experimentally in aligned liquid crystalline films of PFO[6] and has subsequently been derived theoretically.[42] The presence of inert units is also expected to lead to a wider range of exciton hopping times, which would reduce the efficiency of exciton diffusion compared to recombination and thus explain the broader PL linewidth for partially converted (FWHM=0.39 eV) than fully converted (FWHM=0.30 eV) films. Also note that the three Raman modes studied here are located at ($\sim$5 cm^{-1}) higher frequencies in the partially converted samples. This is the opposite trend to that expected if the differences were due exclusively to density variations: Hydrostatic pressure is typically found to shift Raman modes to higher frequencies.[43] The higher frequencies in the partially converted sample are understood rather as being primarily due to a shorter effective conjugation length,[32] a conclusion in agreement with the larger vinylene C=C stretch ($\sim$1621 cm^{-1}) mode intensity for partially converted samples. Therefore, a combination of shorter chain-chain separation distances and more complete elimination of methoxy leaving groups is most likely responsible for the increase in the magnitude of the hole mobility.[44,45]

We also note that a lower effective mass of the charged excited states could be expected as a consequence of close chain packing, especially in crystalline regions of the film. This, in turn, can be expected to contribute to a rise in the overall charge mobility. Because the rigidity of a crystalline lattice restricts the amount of configurational relaxation that can occur in the excited states, or in other words, reduces the electron-geometry coupling constant, the spatial extent of the polaron wave function should increase. We are, however, unable at this stage to quantify the impact that this contribution might have on the TOF charge mobility in PDMeOPV.

Finally, we consider the cause of the increased field dependence of mobility for the fully converted films compared to that for partially converted films. When the GDM is applied to homogeneous systems, stronger positive field dependence can result either from increased disorder in site energies or from reduced disorder in electronic coupling between hopping sites (reduced "configurational" disorder) or from a combination of both.[27] One possible cause of increased field dependence of mobility for the fully converted sample is an increase in site energy disorder due to variations in the electrostatic interactions experienced by the charge transporting units.[27,46] The methoxy side groups and absence of long alkyl side chains in PDMeOPV mean that intermolecular dipolar interactions will be relatively strong and will become stronger at closer chain separations. We propose that in the close interdigitated arrangement adopted by PDMeOPV crystallites, site energy disorder due to dipolar interactions is strong, while the mean electronic interaction is high. In the less dense, partially converted sample, fewer chains adopt the interdigitated configuration so that the mean chromophore separation is larger and the variation in dipolar interactions is reduced. Consequently, the combination of strong dipolar interactions and retained leaving groups offers a plausible explanation for the field dependence data.

V. SUMMARY AND CONCLUSION

We have measured the room-temperature field dependence of the time-of-flight hole mobility in a precursor-route

PDMeOPV. We have compared data for partially converted films with those obtained from films that were crystallized prior to full conversion. Hole mobilities in excess of 10^{-4} cm^2/V s are reported in the latter. PL and Raman micrographs have been studied to give details about the microstructure of the films. The PL images reveal similar features to those seen in the Raman maps and are shown to arise directly from changes in local density. The PL contrast can be explained by a spatial variation in the degree of self-absorption. We believe that the primary mechanism for enhanced self-absorption in denser regions results from scattering-induced elongation of the emitted light's escape path prior to exiting the film. It is shown that the considerably higher hole mobilities in the fully converted sample can be correlated with the appearance of domains of higher density and improved packing of chains in coplanar geometries, leading to higher electronic transfer integrals. The lower mobilities in partially converted films are likely to be influenced by disruption of both the packing geometry and conjugation length by unconverted methoxy leaving group moieties. The more positive field dependence of the mobility in the fully converted samples is explained by increased electrostatic interactions between active chromophores packed into a dense, interdigitated chain arrangement. Our work also demonstrates that ratios of Raman mode intensities (in this case, I_{1280}/I_{1581} for the $\approx$1280 and $\approx$1581 cm^{-1} vibrations of the phenylenevinylene backbone) can readily be used to give an indication of local chain packing in PDMeOPV. Preliminary studies suggest that this finding is valid for other symmetrically substituted dialkoxy PPVs, where we have observed the above ratio to decrease with the alkoxy side-chain length.[28] We are currently seeking to explore the wider applicability of this technique as a simple optical probe to characterize the microscopic transport properties of conjugated polymers and their blends.

ACKNOWLEDGMENTS

We thank the Engineering and Physical Sciences Research Council (UK) (EPSRC) (GR/R97085 "Carbon-based Electronics: A National Consortium") and BP Solar (OSCER Project) for funding. GPC data were provided by the EPSRC-funded polymer characterization service managed and run by RAPRA Technology.

*marc.sims@usa.dupont.com
†d.bradley@imperial.ac.uk

[1] J. H. F. Martens, E. A. Marseglia, D. D. C. Bradley, R. H. Friend, P. L. Burn, and A. B. Holmes, Synth. Met. **55-57**, 449 (1993).
[2] J. H. Burroughes, D. D. C. Bradley, A. R. Brown, R. N. Marks, K. D. Mackay, R. H. Friend, P. L. Burn, and A. B. Holmes, Nature (London) **347**, 539 (1990); R. H. Friend *et al.*, *ibid.* **397**, 121 (1999).
[3] G. Horowitz, Adv. Mater. (Weinheim, Ger.) **10**, 365 (1998); H. Sirringhaus, N. Tessler, and R. H. Friend, Science **280**, 1741 (1998).
[4] R. N. Marks, J. J. M. Halls, D. D. C. Bradley, R. H. Friend, and A. B. Holmes, J. Phys.: Condens. Matter **6**, 1379 (1994).
[5] G. Yu, J. Gao, J. C. Hummelen, F. Wudl, and A. J. Heeger, Science **270**, 1789 (1995); J. J. M. Halls and R. H. Friend, in *Clean Electricity from Photovoltaics*, edited by M. D. Archer and R. D. Hill (Imperial College Press, London, 2001), p. 377.
[6] M. Redecker, D. D. C. Bradley, M. Inbasekaran, and E. P. Woo, Appl. Phys. Lett. **74**, 1400 (1999).
[7] S. A. Choulis, Y. Kim, J. Nelson, D. D. C. Bradley, M. Giles, M. Shkunov, and I. McCulloch, Appl. Phys. Lett. **85**, 3890 (2004).
[8] D. O'Brien, A. Bleyer, D. G. Lidzey, D. D. C. Bradley, and T. Tsutsui, J. Appl. Phys. **82**, 2662 (1997); A. J. Campbell, D. D. C. Bradley, and D. G. Lidzey, *ibid.* **82**, 6326 (1997); A. J. Campbell, M. S. Weaver, D. G. Lidzey, and D. D. C. Bradley, *ibid.* **84**, 6737 (1998); S. J. Martin, D. D. C. Bradley, P. A. Lane, H. Mellor, and P. L. Burn, Phys. Rev. B **59**, 15133 (1999); A. J. Campbell, D. D. C. Bradley, E. Werner, and W. Brütting, Org. Electron. **1**, 21 (2000).
[9] W. Geens, S. E. Shaheen, B. Wessling, C. J. Brabec, J. Poortmans, and N. Serdar Sariciftci, Org. Electron. **3**, 105 (2002).
[10] P. W. M. Blom, Mater. Sci. Eng., R. **27**, 53 (2000); A. R. Inigo, H.-C. Chiu, W. Fann, Y.-S. Huang, U-Ser Jeng, T.-L. Lin, C.-H. Hsu, K.-Y. Peng, and S.-A. Chen, Phys. Rev. B **69**, 075201 (2004).
[11] A. R. Inigo, C. C. Chang, W. Fann, J. D. White, Y. S. Huang, U. S. Jeng, H. S. Sheu, K. Y. Peng, and S. A. Chen, Adv. Mater. (Weinheim, Ger.) **17**, 2147 (2005).
[12] H. C. F. Martens, P. W. M. Blom, and H. F. M. Schoo, Phys. Rev. B **61**, 7489 (2000).
[13] C. H. Tan, A. R. Inigo, W. Fann, P. K. Wei, G. Y. Peng, and S. A. Chen, Org. Electron. **3**, 81 (2002).
[14] U. Jeng *et al.*, Macromolecules **38**, 6566 (2005).
[15] J. H. F. Martens, D. D. C. Bradley, R. H. Friend, E. A. Marseglia, P. L. Burn, and A. B. Holmes, Synth. Met. **41**, 301 (1991); J. H. F. Martens, Ph.D. thesis, University of Cambridge, 1992; J. H. F. Martens, Synth. Met. **55-57**, 440 (1993).
[16] D. D. C. Bradley, J. Phys. D **20**, 1389 (1987); D. D. C. Bradley, R. H. Friend, T. Hartmann, E. A. Marseglia, M. M. Sokolowski, and P. D. Townsend, Synth. Met. **17**, 473 (1987); J. H. F. Martens, D. A. Halliday, E. A. Marseglia, D. D. C. Bradley, R. H. Friend, P. L. Burn, A. B. Holmes, and A. Kraft, *ibid.* **55-57**, 434 (1993).
[17] P. L. Burn, D. D. C. Bradley, A. R. Brown, D. A. Halliday, A. Kraft, R. H. Friend, A. B. Holmes, and J. H. F. Martens, *Electronic Properties of Polymers*, Springer Series in Solid State Sciences Vol. 107 (Springer, Berlin, 1992), p. 293.
[18] T. Granier, E. L. Thomas, D. R. Gagnon, F. E. Karasz, and R. W. Lenz, J. Polym. Sci., Part B: Polym. Phys. **24**, 2793 (1986).
[19] J. H. F. Martens, D. A. Halliday, E. A. Marseglia, D. D. C. Bradley, R. H. Friend, P. L. Burn, and A. B. Holmes, Synth. Met. **55**, 434 (1993).
[20] (a) H. Liem, P. Etchegoin, K. S. Whitehead, and D. D. C. Bradley, Adv. Funct. Mater. **13**, 66 (2003); (b) M. Sims, K. Zheng, M. Campoy-Quiles, R. Xia, P. N. Stavrinou, and D. D. C. Bradley, J. Phys.: Condens. Matter **17**, 6307 (2005); (c) M. C. Gather and

D. D. C. Bradley, Adv. Funct. Mater. **17**, 479 (2007).
[21] P. L. Burn, D. D. C. Bradley, R. H. Friend, D. A. Halliday, A. B. Holmes, R. W. Jackson, and A. Kraft, J. Chem. Soc., Perkin Trans. 1 **1992**, 3225.
[22] F. Papadimitrakopoulos, M. Yan, L. Rothberg, H. Katz, and M. E. Galvin, Mol. Cryst. Liq. Cryst. Sci. Technol., Sect. A **256**, 663 (1994).
[23] M. Campoy-Quiles, G. Heliotis, R. D. Xia, M. Ariu, M. Pintani, P. Etchegoin, and D. D. C. Bradley, Adv. Funct. Mater. **15**, 925 (2005).
[24] H. S. Woo, O. Lhost, S. C. Graham, D. D. C. Bradley, R. H. Friend, C. Quattrocchi, J.-L. Brédas, R. Schenk, and K. Müllen, Synth. Met. **59**, 13 (1993).
[25] H. S. Woo, S. C. Graham, D. A. Halliday, D. D. C. Bradley, R. H. Friend, P. L. Burn, and A. B. Holmes, Phys. Rev. B **46**, 7379 (1992).
[26] E. Lebedev, Th. Dittrich, V. Petrova-Koch, S. Karg, and W. Brütting, Appl. Phys. Lett. **71**, 2686 (1997).
[27] H. Bässler, Phys. Status Solidi B **175**, 15 (1993); P. M. Borsenberger and D. S. Weiss, *Organic Photoreceptors for Xerography* (Dekker, New York, 1993).
[28] S. M. Tuladhar, M. Sims, J. Kirkpatrick, R. C. Maher, A. J. Chatten, D. D. C. Bradley, J. Nelson, C. B. Nielsen, P. Massiot, W. George, and J. H. G. Steinke (unpublished).
[29] (a) H. Liem, P. Etchegoin, K. S. Whitehead, and D. D. C. Bradley, J. Appl. Phys. **92**, 1154 (2002); (b) H. Liem, P. Etchegoin, and D. D. C. Bradley, Phys. Rev. B **64**, 144209 (2001).
[30] N. Colthup, L. Daly, and S. Wiberley, *Introduction to Infrared and Raman Spectroscopy*, 3rd ed. (Academic, London, 1990).
[31] X. Wu, G. Shi, L. Qu, J. Zhang, and F. Chen, J. Polym. Sci., Part A: Polym. Chem. **41**, 449 (2003).
[32] A. Sakamoto, Y. Furukawa, and M. Tasumi, J. Phys. Chem. **96**, 1490 (1992).
[33] The fact that the FWHM and frequency of the 1305 and 1280 cm^{-1} modes are observed to undergo parallel variations to those of the quadrant ring stretch in the dense and/or ordered regions might suggest that interchain registration is not just limited to the rings but also extends along the backbones.
[34] As with FWHM and Raman shift data, the use of Raman intensity *ratios* to provide imaging contrast has a number of advantages over a simple monitor of the absolute intensity of a single mode. It avoids problems that can arise from heterogeneities at the film surface leading, for instance, to defocusing during lateral stage translation, or from inhomogeneities in film thickness leading to changes in scattering volume.
[35] R. Mahrt, J. Yang, A. Greiner, H. Bässler, and D. D. C. Bradley, Makromol. Chem., Rapid Commun. **11**, 415 (1990).
[36] S. Heun, R. F. Mahrt, A. Greiner, U. Lemmer, H. Bässler, D. A. Halliday, D. D. C. Bradley, P. L. Burn, and A. B. Holmes, J. Phys.: Condens. Matter **5**, 247 (1993).
[37] J.-L. Brédas, D. Beljonne, V. Coropceanu, and J. Cornil, Chem. Rev. (Washington, D.C.) **104**, 4971 (2004).
[38] M. Ariu, D. G. Lidzey, and D. D. C. Bradley, Synth. Met. **111-112**, 607 (2000).
[39] E. M. Conwell, Trends Polym. Sci. **5**, 218 (1997).
[40] J. B. Birks, *Photophysics of Aromatic Molecules* (Wiley Interscience, New York, 1970).
[41] M. Sims, K. Zheng, and D. D. C. Bradley (unpublished).
[42] S. Athanasopoulos, J. Kirkpatrick, D. Martınez, J. M. Frost, C. M. Foden, A. B. Walker, and J. Nelson (unpublished).
[43] S. Guha and M. Chandrasekhar, Phys. Status Solidi B **241**, 3318 (2004).
[44] A. J. Chatten, S. M. Tuladhar, and J. Nelson, Proceedings of the 31st IEEE Photovoltaic Specialists' Conference, Florida, 2005, pp. 31–36.
[45] J. Nelson (unpublished).
[46] D. H. Dunlap, P. E. Parris, and V. M. Kenkre, Phys. Rev. Lett. **77**, 542 (1996).